

1 **A new temperature-photoperiod coupled phenology module in LPJ-**
2 **GUESS model v4.1: optimizing estimation of terrestrial carbon and**
3 **water processes**

4 Shouzhi Chen¹, Yongshuo H. Fu^{1,2*}, Mingwei Li¹, Zitong Jia¹, Yishuo Cui¹, Jing
5 Tang^{3*}

6 ¹College of Water Sciences, Beijing Normal University, Beijing 100875, China.

7 ²Plants and Ecosystems, Department of Biology, University of Antwerp, Antwerp,
8 Belgium.

9 ³Center for Volatile Interactions, Department of Biology, University of Copenhagen,
10 Denmark.

11

12 *Corresponding author:*

13 Yongshuo Fu (yfu@bnu.edu.cn); Jing Tang (jing.tang@bio.ku.dk).

14 **Abstract**

15 Vegetation phenological shifts impact the terrestrial carbon and water cycle and
16 contribute to affecting local climate system through biophysical and biochemical
17 processes. Dynamic Global Vegetation Models (DGVMs), serving as pivotal simulation
18 tools for investigating climate impacts on terrestrial ecosystem processes, incorporate
19 representations of vegetation phenological processes. Nevertheless, it is still a challenge
20 to achieve accurate simulation of vegetation phenology in the DGVMs. Here, we
21 developed and implemented spring and autumn phenology models into one of the
22 DGVMs, LPJ-GUESS. The new phenology modules are driven by temperature and
23 photoperiod, and are parameterized for deciduous trees and shrubs by using remote
24 sensed phenological observations and the reanalysis data ERA5. The results show that

25 the LPJ-GUESS with the new phenology modules substantially improved the accuracy
26 in capturing start and end dates of growing seasons. For the start of the growing season,
27 the simulated RMSE for deciduous trees and shrubs decreased by 8.04 and 17.34 days,
28 respectively. For the autumn phenology, the simulated RMSE for deciduous tree and
29 shrubs decreased by 22.61 and 17.60 days, respectively. Interestingly, we have also
30 found that differences in simulated start and end of the growing season also alter the
31 simulated ecological niches and competitive relationships among different plant
32 functional types (PFTs), and subsequently influence the terrestrial carbon and water
33 cycles. Hence, our study highlights the importance of accurate phenology estimation to
34 reduce the uncertainties in plant distribution and terrestrial carbon and water cycling.

35 **Keywords:** LPJ-GUESS, phenology model, model modification, ecological processes

36 **1. Introduction**

37 Vegetation plays a pivotal role within the terrestrial ecosystem, as the interplay
38 between vegetation and climate exerts significant influence on the mass and energy
39 cycles across a broad range of temporal and spatial scales (Zhu et al., 2016; Piao et al.,
40 2019; Chen et al., 2022a). In recent years, with the increase of carbon dioxide
41 concentration and land surface temperature, significant vegetation greening has been
42 reported world widely, and the annual growth dynamics of vegetation have undergone
43 significant changes, especially the spring and autumn phenological changes (Zhu et al.,
44 2016). A large amount of research evidences have indicated that climate change results
45 in the advancement of spring phenology and the postponement of autumn phenology,
46 exerting a profound influence on the carbon and water cycles within terrestrial
47 ecosystems (Piao et al., 2019; Badeck et al., 2004; Zhou et al., 2020), and the
48 geographic distribution of species (Chuine, 2010; Fang and Lechowicz, 2006; Huang
49 et al., 2017). Under conditions of sufficient water supply and no radiation constraints,
50 the extension of the growing season resulting from vegetation phenological shifts will
51 contribute additional carbon sinks to terrestrial ecosystems (Zhang et al., 2020; Keenan
52 et al., 2014). Longer growing seasons also lead to greater evapotranspiration, mainly in
53 early spring and autumn, which in turn reduces watershed runoff (Huang et al., 2017;
54 Kim et al., 2018; Chen et al., 2022b; Geng et al., 2020). Nevertheless, it is still a
55 challenge to achieve accurate simulation of vegetation phenology in dynamic global
56 vegetation models (DGVMs), especially in the context of climate change (Richardson
57 et al., 2012). We urgingly caution that improving the vegetation phenology module of

58 DGVMs, and taking the response of vegetation phenology to climate change into
59 consider comprehensively, which is a necessary development to improve model
60 simulation accuracy and reduce model uncertainty.

61 The State-of-the-art DGVMs generally include phenology modules in vegetation
62 submodels, but the implementations vary widely, which include: 1) Using fixed and
63 prescribed seasonal dynamics to characterize phenology, and the models using this
64 method include SiB model, SiBCASA model, ISAM model, etc. (Sellers et al., 1986;
65 Schaefer et al., 2008; Jain and Yang, 2005). 2) Using remote sensing data or in-situ
66 observations directly describing the vegetation growth dynamics instead of process-
67 based simulation, SiB2, BEPS and ED2 are all based on this method to describe the
68 vegetation growth dynamics (Sellers et al., 1996; Deng et al., 2006; Medvigy et al.,
69 2009). 3) Using vegetation phenology model which take the response of vegetation
70 biophysiology to environment factors into account to simulate vegetation growth
71 dynamics. In comparison to the first two methods, the third approach offers the
72 advantage of depicting the responses of vegetation to the external environment
73 grounded in plant physiological processes , and can trace the dynamics of vegetation
74 growth amidst changing environment conditions, so it is adopted by several DGVMs,
75 e.g. Biome-BGC, ORCHIDEE and LPJ-GUESS (Thornton et al., 2002; Krinner et al.,
76 2005; Sitch et al., 2003). With the evolving comprehension of the intricate response
77 mechanisms of vegetation to external environment, vegetation phenological models
78 have experienced substantial advancements in recent decades, which encompass shifts
79 from single-process to multi-process mechanisms and from single-variable to multi-

80 factor model constraints. (Liu et al., 2018a; Fu et al., 2020; Piao et al., 2019). For spring
81 phenological models, in the early stage, temperature was the only factor considered,
82 resulting in relatively simplistic model processes, which was also commonly adopted
83 by DGVMs (GDD and Unified etc.) (Sarvas, 1972; Chuine, 2000). With the deepening
84 of the understanding of spring phenological mechanism, factors such as radiation and
85 photoperiod have been introduced into the phenological model, and the corresponding
86 complex regulatory mechanisms have also been perfected, e.g. Sequential model,
87 Parallel model and DORMPHOT model etc. (Hänninen, 1990; Kramer, 1994; Caffarra
88 et al., 2011). As for the autumn phenological model, the early model form was also
89 relatively simple (cold temperature-driven CDD model) but widely used in DGVMs,
90 and some DGVMs used fixed leaf longevity for determination of autumn phenological
91 dates. The development of relatively complex autumn phenological mechanism models
92 is relatively late, and these advanced autumn phenological models take photoperiod and
93 carbon accumulation into account in the model process, such as temperature-
94 photoperiod bioclimatic (DM) model, photosynthesis-influenced autumn phenology
95 (PIA) model (Zani et al., 2020; Delpierre et al., 2009). Many researches have pointed
96 out that early phenological models tend to be overly simplistic and result in biased
97 predictions, which indicates that the vegetation phenological models of DGVMs need
98 to be updated urgently (Kucharik et al., 2006; Ryu et al., 2008). The use of more
99 accurate phenological models covering more complex mechanisms is of great
100 significance to reduce the simulation errors of DGVMs and improve the simulation
101 reliability under future climate warming.

102 In this study, we used the remote sensing-based phenology data and the threshold
103 and maximum change rate methods to parameterize the spring DORMPHOT model and
104 autumn DM model. This was applied specifically for boreal needle leaved summergreen
105 tree (BNS), Shade-intolerant broadleaved summergreen tree (IBS), shade-tolerant
106 temperate broadleaved summergreen tree (TeBS) and summergreen shrubs plant
107 function types (PFTs). The new phenology module with these parameters were coupled
108 into the LPJ-GUESS model. The objectives of this study are as follows:1) to couple
109 more mechanistic phenology modules into LPJ-GUESS to improve the accuracy of
110 spring and autumn phenology simulations; (2) to assess the impacts of different
111 vegetation phenological algorithms on the carbon and water process simulations.

112 **2. Materials and methods**

113 **2.1 Datasets**

114 **2.1.1 GIMMS NDVI_{4g}**

115 Normalized differential vegetation index (NDVI) is commonly used as a proxy for
116 vegetation canopy greenness and growth condition. In the study, we used the forth-
117 generation NDVI dataset of GIMMS, which provides biweekly NDVI records with a
118 spatial resolution of $1/12^\circ$ (~8 km), during 1982-2017 to extract the start and end of
119 growing season (Pinzon and Tucker, 2014; Tucker et al., 2005; Cao et al., 2023). This
120 NDVI dataset has been refined and corrected for orbital drift, calibration, viewing
121 geometry, and volcanic aerosols, which can accurately reflect the accurate growth
122 dynamics of surface vegetation (Kaufmann et al., 2000).

123 **2.1.2 Climate forcing field data**

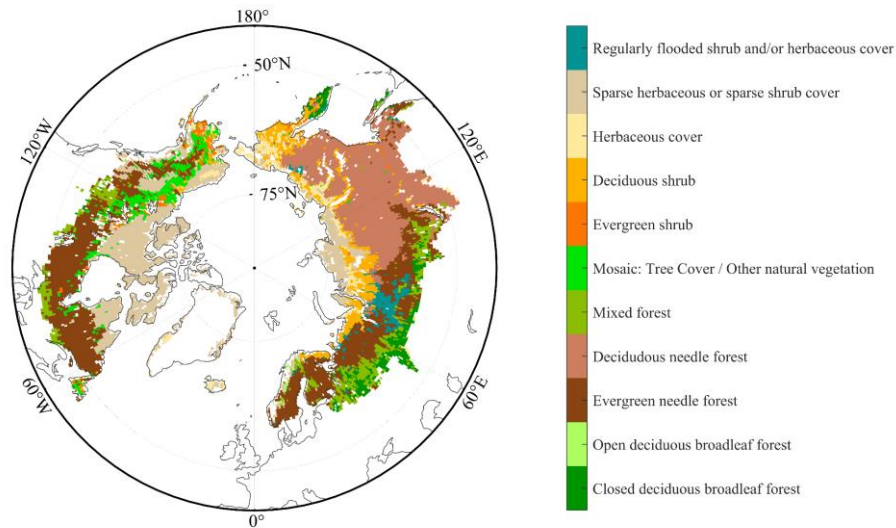
124 We used CRU-NCEP V7 data with a horizontal spatial resolution of $0.5^\circ \times 0.5^\circ$ as
125 the forcing field data for driving the LPJ-GUESS model during 1901-2015. The forcing
126 field data include monthly air temperature (1901-1978) and precipitation, wind speed,
127 wet days, incoming shortwave radiation and relative humidity over the period 1901-
128 2015, which can be downloaded from <https://rda.ucar.edu/datasets/ds314.3/>. The
129 ERA5-Land daily air temperature dataset has been used to parameterize spring and
130 autumn phenological algorithms and force LPJ-GUESS model. The dataset is a global
131 reanalysis dataset developed by the European Centre for Medium-Range Weather
132 Forecasts (ECMWF), which utilises advanced data assimilation techniques combining
133 observations from various sources, such as satellites, weather stations, and weather
134 balloons, with numerical weather prediction models. We downloaded the ERA5 land
135 daily air temperature at 0.5° spatial resolution (consistent with CRU NCEP V7 data,
136 from 1979-2015) from their official website
137 (<https://cds.climate.copernicus.eu/cdsapp#!/dataset/reanalysis-era5-land?tab=form>).

138 Due to possible bias between different data sets, we calculated the monthly average of
139 ERA5 land daily air temperature and calculated its climatology, as well as climatology
140 of CRU NCEP v7 monthly air temperature data, and corrected the bias of ERA5 land
141 data according to the deviation.

142 **2.1.3 GLC 2000 land cover data**

143 Satellite remote sensing can capture the collective information from mixed pixels

144 comprised of various plants and also information from dominant vegetation. The data
 145 acquired through satellite remote sensing can be regarded as representative of a
 146 particular vegetation type only when the plant functional types within a gridcell exhibit
 147 a relatively homogeneous composition. Based on GLC2000 land cover types data,



148 which are designated according to PFTs ascribed to satellite images and ground-truth
 149 by regional analysts with 1 km spatial resolution (Bartholome and Belward, 2005), we
 150 calculated the proportion of different PFTs in the $0.5^\circ \times 0.5^\circ$ gridcell to identify pixels
 151 dominated by a specific plant functional type (the proportion of a specific plant function
 152 type is greater than 50%, Fig. 1 and Fig. S1).

153 **Figure 1. The spatial distributions of 11 detailed regional land-cover types in the**
 154 **GLC2000 products.** BNS: Deciduous needle forest, IBS&TeBS: Open deciduous
 155 broadleaf forest and closed deciduous broadleaf forest, Shrubs: Sparse herbaceous or
 156 sparse shrub cover and Deciduous shrub.

157
 158 **2.1.4 VPM GPP and REA ET data**

159 We used the vegetation photosynthesis model (VPM) gross primary productivity
 160 (GPP) (Zhang et al., 2017) and REA ET (Lu et al., 2021) to compare the simulation
 161 results of carbon and water fluxes with the LPJ-GUESS model.

162 The VPM GPP dataset is constructed upon an enhanced light use efficiency theory,
163 utilizing satellite data from MODIS and climate data from NCEP Reanalysis II. It
164 incorporates an advanced vegetation index (VI) gap-filling and smoothing algorithm,
165 along with distinct considerations for C3/C4 photosynthesis pathways. VPM GPP
166 product can be download from [https://data.nal.usda.gov/dataset/global-moderate-
167 resolution-dataset-gross-primary-production-vegetation-2000%E2%80%932016](https://data.nal.usda.gov/dataset/global-moderate-resolution-dataset-gross-primary-production-vegetation-2000%E2%80%932016).

168 ERA ET is a combination of three existing model-based products – the fifth-
169 generation ECMWF reanalysis (ERA5), Global Land Data Assimilation System
170 Version 2 (GLDAS2), and the second Modern-Era Retrospective analysis for Research
171 and Applications (MERRA-2), which using the reliability ensemble averaging (REA)
172 method, minimizing errors using reference data, to combine the three products over
173 regions with high consistencies between the products using the coefficient of variation
174 (CV). The REA ET data can be accessed at <https://doi.org/10.5281/zenodo.4595941> (Lu
175 et al., 2021).

176 **2.2 Phenology dates extraction**

177 We used five phenological extraction methods, which includes three threshold-
178 based methods (i.e. Gaussian-Midpoint, Spline-Midpoint and Timesat-SG Methods)
179 and two change rate-based methods (i.e. the HANTS-Maximum and Polyfit-Maximum
180 methods) following previous studies (Cong et al., 2012; Savitzky and Golay, 1964;
181 Chen et al., 2023), to retrieval spring (start of growing season, SOS) and autumn (end
182 of growing season, EOS) phenological events (Fig.S2). Phenological extraction based
183 on multiple methods consists of three steps: 1) smoothing and interpolating the NDVI

184 date to obtain the smooth and continuous NDVI daily time series; 2) using the threshold
185 value (0.5 for SOS and 0.2 for EOS) or the maximum rate of change to extract the
186 vegetation phenology from each single method (Reed et al., 1994; White et al., 1997;
187 White et al., 2009; Piao et al., 2006); 3) averaging the phenological results obtained by
188 different extraction methods to reduce uncertainties associated with a single method
189 (Due to the different fitting methods, interpolation methods and threshold settings of
190 different extraction methods) (Fu et al., 2021; Fu et al., 2023).

191 **2.3 Model description**

192 LPJ-GUESS is a process-based dynamic global vegetation model that can
193 simulate vegetation dynamics and soil biogeochemical processes across different
194 terrestrial ecosystems. At gridcell level, the model simulates vegetation growth,
195 allometry competition, mortality and disturbances (Sitch et al., 2003; Morales et al.,
196 2005; Hickler et al., 2004). The PFTs within the framework of the LPJ-GUESS model
197 encapsulate the extensive spectrum of structural and functional attributes
198 characteristic of potential plant species. Within a given area (patch, corresponding in
199 size approximately to the maximum area of influence of one large adult individual on
200 its neighbors), plant growth is governed by the synergistic interplay of bioclimatic
201 constraints and interspecific competition for spatial dominance, access to light, and
202 vital resources. In a gridcell (stand), it's typically simulating multiple such patches
203 to represent different disturbance histories within a landscape, and across these
204 patches, the modeled properties tend to coalesce towards a singular, overarching
205 average value.

206 In LPJ-GUESS model, spring phenology is calculated based on spring heat and
207 winter cold requirements (Sykes et al., 1996). Plants have certain energy
208 requirements for budburst, which are expressed by using growing degree days above
209 5 degrees (GDD5), while growing degree days to budburst is also related to the length
210 of the chilling period. An increase in chilling periods can reduce the requirement for
211 growing degree days to budburst, in other words, budburst can be delayed long
212 enough to minimize the risk that the emerging buds will be damaged by frost
213 (Equation 1):

$$GDD = a + b \times e^{-k \times C} \quad (1)$$

214 Where a, b and k are PFT-specific constants, and C is the length of chilling
215 period. GDD represents the growing degree days requirement of a specific PFT at a
216 chilling period length of C. Growing degree days are defined as the accumulation of
217 temperatures above the base temperature (generally 5 °C), and the length of chilling
218 period is defined as the days that daily mean temperature below 5 °C.

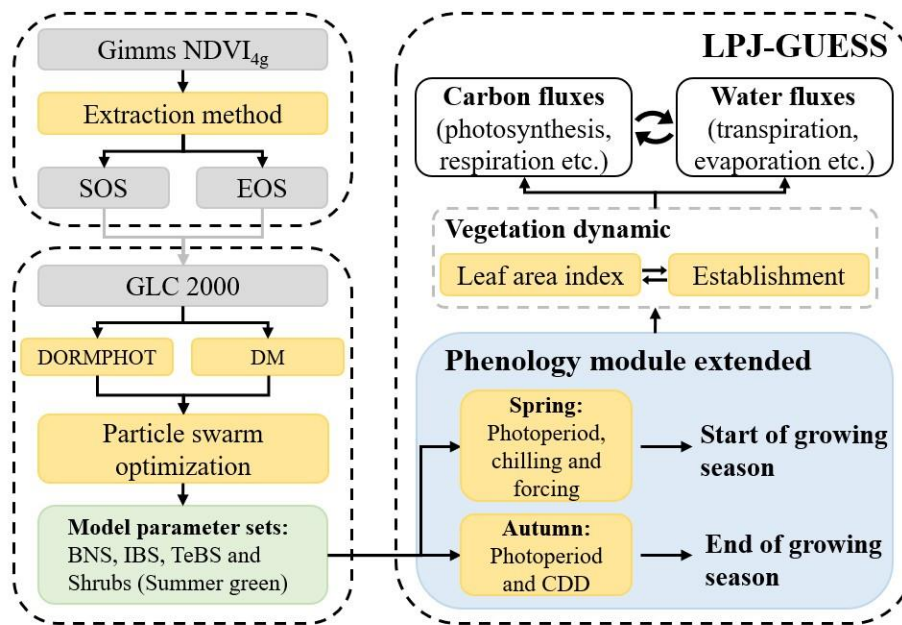
219 For autumn phenology, leaf longevity was used as a threshold in the LPJ-
220 GUESS model for the simple prediction of senescence. It is assumed in the model
221 that autumn phenology occurs when the cumulative complete leaf longevity is greater
222 than 210 days or the daily average temperature below 5°C in autumn.

223 Within each stand, 50 different patches (in this study) were applied to represent
224 different disturbance histories within a landscape. The simulations over the study
225 areas included 23 PFTs, which consist of five grass, three bryophytes, eight shrubs
226 and seven tree PFTs, and the summergreen PFTs involved in the improvement of

227 vegetation phenological simulation contain BNS, IBS, TeBS and deciduous shrubs
 228 (hereafter called Shrubs), see detailed description in (Tang et al., 2023) and Rinnan
 229 et al. (2020).

230 2.4 LPJ-GUESS phenology module extension

231 We improved the spring and autumn phenological modules of the LPJ-GUESS
 232 model by coupling DORMPHOT model and DM model into LPJ-GUESS according to
 233 the phenological module improvement flow chart (Fig.2).



234 **Figure 2 Flowchart of spring and autumn phenological module extension in LPJ-**
 235 **GUESS.** Dotted boxes represent independent work, gray boxes represent different data
 236 sets or intermediate process results, and yellow boxes represent different calculation
 237 methods or model modules. CDD, cold degree days.

238 The spring phenological model in LPJ-GUESS was replaced by DORMPHOT
 239 model, which introduces the effect of photoperiod on dormancy. This model refines the
 240 spring phenological model into three stages: dormancy induction, dormancy release and
 241 growth resumption (Caffarra et al., 2011). The dormancy induction process is triggered

242 by a short photoperiod (DR_P) and a low temperature (DR_T), and finishes when the
 243 cumulant of the product of DR_P and DR_T reaches a specific threshold ($DS > D_{crit}$,
 244 Equation 2, 3 and 4):

$$DS = \sum_{t_0}^t DR_T \times DR_P \quad (2)$$

$$DR_T = \frac{1}{1 + e^{aD \times (T - bD)}} \quad (3)$$

$$DR_P = \frac{1}{1 + e^{10 \times (DL - DL_{crit})}} \quad (4)$$

245 Where t_0 is the start date of dormancy induction, which defined at September 1st
 246 of the year preceding budburst, DS represents the state of dormancy induction (the
 247 cumulant of daily photoperiod, i.e. DR_P , and temperature, i.e. DR_T , effect), T is the
 248 daily mean temperature, and DL is day length on day t . aD , bD and DL_{crit} are model
 249 parameters that regulate the effect of photoperiod and temperature.

250 Dormancy release and growth resumption start after dormancy induction is
 251 complete (t_d), which represent a parallel chilling and forcing process, respectively. The
 252 total daily rate of chilling (S_C) is defined as the accumulation of daily chilling (R_C) as
 253 Equation 5, and the daily forcing (R_f) is determined by both photoperiod and S_C
 254 (Equation 6, 7 and 8), that the effect of photoperiod and chilling on R_f counteracts each
 255 other. The increase of photoperiod will decrease R_f while the increase of chilling will
 256 reverse the effect:

$$S_c = \sum_{t_d}^t R_c = \sum_{t_d}^t \frac{1}{1 + e^{aC \times (T - cC)^2 + (T - cC)}} \quad (5)$$

$$DL_{50} = \frac{24}{1 + e^{hDL \times (S_c - C_{crit})}} \quad (6)$$

$$T_{50} = \frac{60}{1 + e^{gT \times (DL - DL_{50})}} \quad (7)$$

$$S_f = \sum_{t_d}^t R_f = \sum_{t_d}^t \frac{1}{1 + e^{dF \times (T - T_{50})}} \quad (8)$$

257 Where aC , cC and C_{crit} are the model parameters of chilling process, and hDL , gT
258 and dF are the model parameters of forcing process. When the total daily rate of forcing
259 (S_f) reaches a critical value F_{crit} , vegetation completely resumes growth and spring
260 phenological events occurred. Note that gT and hDL must be greater than zero to limit
261 the monotonicity of Equation 6 and 7.

262 Since the lack of process based submodule to simulate autumn phenology in LPJ-
263 GUESS model, and only a fixed leaf longevity is used to define occurrence date of
264 autumn phenology, we introduced autumn phenology process that considers
265 photoperiod and cold temperature effects by coupling the DM model into the LPJ-
266 GUESS model (Delpierre et al., 2009). The DM model assumes that plants will respond
267 to low temperature (below base temperature, T_b) only when the photoperiod is below a
268 critical value (DL_{crit}), and the daily rate of senescence (R_{sen}) on that day is determined
269 by cold temperature and photoperiod (Equation 9,10 and 11):

$$f(DL) = \alpha_{pn} \times \frac{DL}{DL_{crit}} + (1 - \alpha_{pn}) \times \left(1 - \frac{DL}{DL_{crit}}\right), \quad \alpha_{pn} \in \{0,1\} \quad (9)$$

$$R_{sen} = \begin{cases} 0, & DL \geq DL_{crit} \\ 0, & DL < DL_{crit} \text{ \& } T \geq T_b \\ (T_b - T)^x \times f(DL)^y, & DL < DL_{crit} \text{ \& } T < T_b \end{cases} \quad (10)$$

$$S_{sen} = \sum_{t_0}^t R_{sen} \quad (11)$$

270 Where α_{pn} is a parameter determines that photoperiod shorter than the DL_{crit}
 271 threshold weaken (α_{pn} equal to 1) or strength (α_{pn} equal to 0) the cold-degree sum effect.
 272 x and y are the indices of the temperature and photoperiod terms in the formula, which
 273 are used to adjust the degree of influence of temperature and photoperiod on R_{sen} ,
 274 respectively.

275 2.5 Phenological model parameterization

276 Utilizing the spatial distribution of predominantly homogeneous pixels
 277 corresponding to distinct vegetation types, we partitioned the remote sensing
 278 phenological dataset, and finally obtained the phenological dataset of BNS, IBS, TeBS
 279 and Shrubs for the parameterization of DORMPHOT and DM models. We divided the
 280 phenology dataset into two parts according to the odd or even number of years, the odd-
 281 numbered years for model parameter internal calibration and the even-numbered years
 282 for model external calibration. Particle swarm optimization (PSO) algorithm was
 283 applied to parameterize the DORMPHOT and DM model for different PFTs, which
 284 used the mixed function that comprehensively considers multiple evaluation indicators

285 as the objective function ($f(mixed)$, Equation 12), and sets the upper limit of iteration
286 to 5000 times to find the global optimal parameter (Marini and Walczak, 2015; Poli et
287 al., 2007). The parameters of DORMPHOT model and DM model applicable to BNS,
288 IBS&TeBS and Shrubs PFTs were found by PSO algorithm (Table S1 and S2).

$$f(mixed) = 100*(1-R^2)+100*(1-NSE)+10*RMSE \quad (12)$$

289 Where R^2 is coefficient of determination, NSE is Nash–Sutcliffe Efficiency, and
290 RMSE is Root mean square error. The coefficients in front of each term of the formula
291 are used to adjust the weights of different evaluation indicators. The smaller the
292 objective function, the closer the simulated value of the model is to the observed value.

293 **2.6 Simulation set-up**

294 To compare the simulation performance of LPJ-GUESS which employing original
295 phenological module and modified phenological module (the extended LPJ-GUESS).
296 We first ran the model using CRU NCEP v7 gridded climate data over the period 1901-
297 1978 with a 500 year spin up, and saved all model state variables at the end of 1978
298 (used the original phenological module, and the status variables associated with the
299 extended phenological module were also updated and saved concurrently). Avoiding
300 the differences in the simulated vegetation and soil state variables outside the study
301 period, i.e. 1979-2015 (Viovy, 2018). Then we restarted the model simulations
302 (applying the original phenological module and extended phenological module,
303 respectively) with the saved model state variables at the last day of 1978 and ERA5
304 land daily air temperature, note that other forcing data were still from CRU NCEP v7

305 data set, and printed start (end) of growing season of summer green PFTs, monthly grid
 306 level GPP and actual evapotranspiration (AET) of each PFT and foliar projection cover
 307 (FPC), for investigating the simulation difference which induced by phenological
 308 simulation differences. All the data processing and analysis in this study were
 309 completed in matlab 2020b (www.mathworks.com).

310

311 **3. Results**

312 **3.1 Phenology simulation performance**

313 For spring phenology, DORMPHOT model has the best simulation performance
 314 in the IBS&TeBS region ($R^2 = 0.62$ & $NSE = 0.62$), followed by in the regions
 315 dominated by BNS ($R^2 = 0.52$ & $NSE = 0.52$) and Shrubs ($R^2 = 0.47$ & $NSE = 0.47$)
 316 (Table 1). For autumn phenology the simulation performance was generally worse than
 317 that of spring phenology. The DM model has the best simulation performance in the
 318 Shrubs region, ($R^2 = 0.39$ & $NSE = 0.39$), followed by in the regions dominated by
 319 BNS ($R^2 = 0.33$ & $NSE = 0.32$) and IBS&TeBS ($R^2 = 0.47$ & $NSE = 0.47$) (Table 1).

320 **Table 1 Model performances of DORMPHOT and DM models.**

Model	Plant function type	Internal calibration			External calibration		
		R^2	NSE	RMSE	R^2	NSE	RMSE
DORMPHOT	BNS	0.54	0.53	7.71	0.52	0.52	7.96
	IBS&TeBS	0.61	0.61	7.92	0.62	0.62	7.91
	Shrub	0.45	0.44	11.3	0.47	0.47	11.1
DM	BNS	0.28	0.28	10.7	0.33	0.32	10.7
	IBS&TeBS	0.29	0.28	14.9	0.32	0.31	14.4
	Shrub	0.42	0.42	10.4	0.39	0.39	10.5

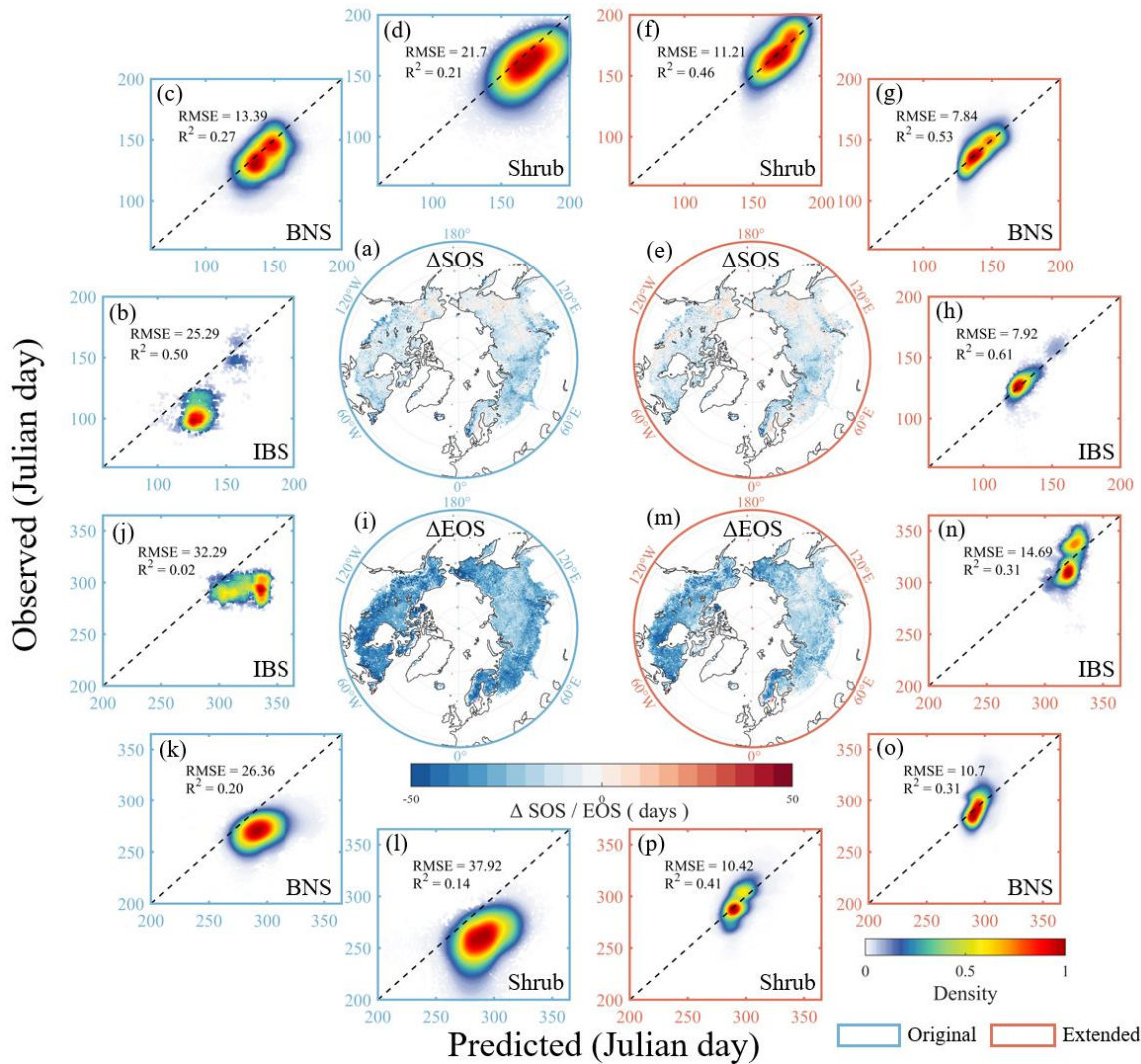
321 R^2 , coefficient of determination, NSE, Nash–Sutcliffe Efficiency, RMSE, Root mean
322 square error. BNS, boreal needle leaved summergreen tree, IBS, Shade-intolerant
323 broadleaved summergreen tree, TeBS, shade-tolerant temperate broadleaved
324 summergreen tree and Shrubs, summergreen shrubs plant function types.
325

326 Compared with remote sensing-based vegetation phenological indices, LPJ-
327 GUESS with the original phenological module estimated earlier spring onset and
328 autumn leaf senescence. The simulated spring phenology matches better than that of
329 autumn phenology. The extended LPJ-GUESS model has greatly improved the
330 estimation accuracy in regions dominated by BNS, IBS&TeBS and Shrubs PFTs (Fig.
331 3 and Fig. S3). For spring phenology, the simulated R^2 (RMSE) of the extended LPJ-
332 GUESS model for regions dominated by BNS, IBS&TeBS and Shrubs PFTs were 0.53
333 (7.84), 0.61 (7.92) and 0.46 (11.21), respectively, which increased (decreased) by 0.26
334 (5.55), 0.12 (17.34) and 0.25 (10.53) compared with the original phenological module.

335 We found that PFTs with larger R^2 increase in spring phenological simulation also
336 had smaller RMSE reductions for the extended model, indicating the improvements in
337 capturing interannual change and the multi-year mean value. The autumn phenology
338 simulation performance with was greatly improved by integrating DM model for
339 regions dominated by BNS, IBS&TeBS and Shrubs PFTs, the simulated R^2 (RMSE) of
340 the extended LPJ-GUESS model were 0.31 (10.70), 0.31 (14.69) and 0.41 (10.42),
341 respectively, which increased (decreased) by 0.11 (15.66), 0.31 (17.60) and 0.27 (27.50).
342 By comparing the LPJ-GUESS simulated daily LAI before and after coupling the DM
343 model, we also found that the autumn LAI values simulated by the extended LPJ-
344 GUESS no longer suddenly decrease to 0 over a day, but rather smoothly decrease with

345 the sigmoid function according to the control of cold temperature and photoperiod (Fig.
346 S4).

347 We also used two calibration schemes to explore the phenology simulation
348 performance of the original phenological module of LPJ-GUESS after parameterization.
349 The first one is based on the original LPJ-GUESS model to determine a common
350 parameter set of all deciduous tree PFTs, and the second one is to determine a unique
351 set of parameters for each PFTs. The results show that the phenology simulation
352 performance of the original phenological module under the two calibration schemes
353 was inferior to that of the new phenological module based on the cooperative control
354 of temperature and photoperiod (Table S3)

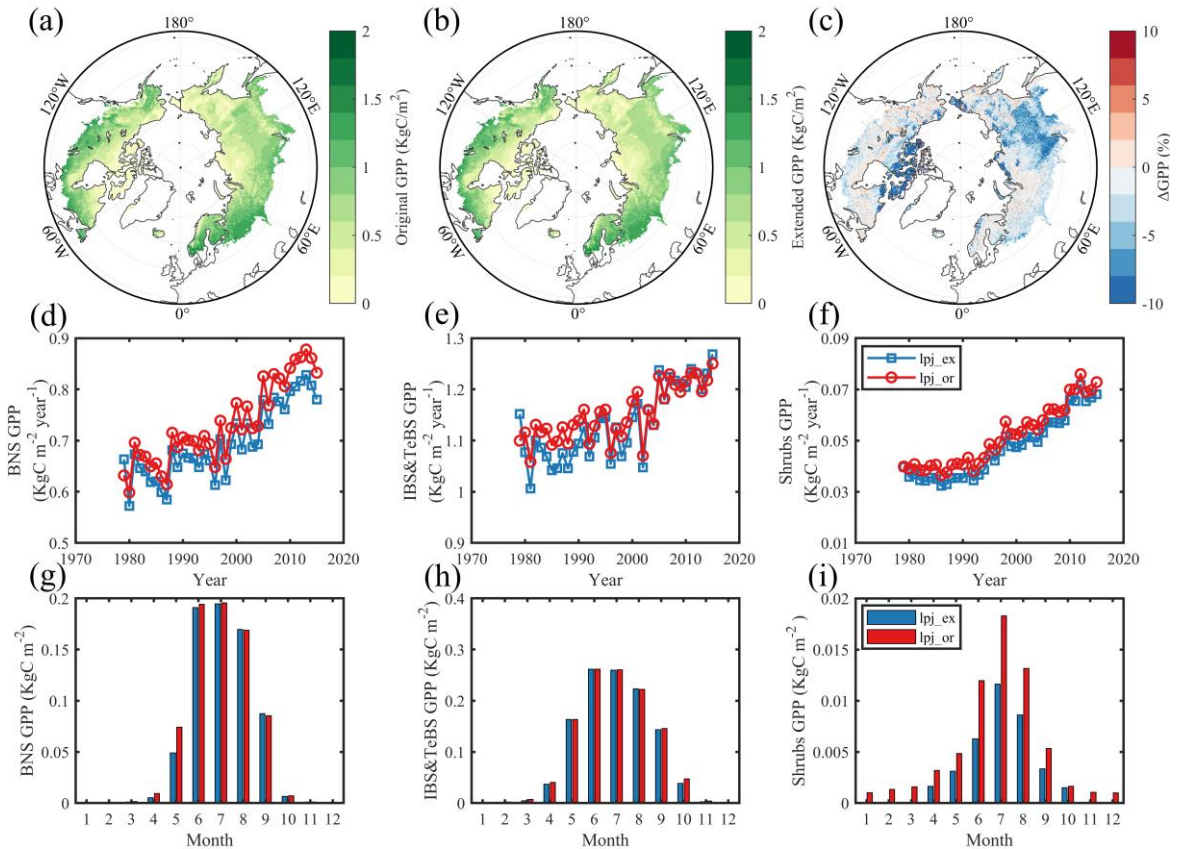


355 **Figure 3 Comparison of the simulated performance of spring (SOS) and autumn**
 356 **(EOS) phenology between the original (left blue panels) and the extended (right**
 357 **red panels) LPJ-GUESS. (a-d) Simulation performance of SOS using the original**
 358 **LPJ-GUESS, (e-h) Simulation performance of SOS using the extended LPJ-GUESS,**
 359 **(i-l) Simulation performance of EOS using the original LPJ-GUESS, (m-p) Simulation**
 360 **performance of EOS using the extended LPJ-GUESS. Blue and red boxes represent**
 361 **spring and autumn phenological simulations. The spatial geographic map showed the**
 362 **difference between the simulation results of LPJ-GUESS model and the remote sensing**
 363 **phenology, with blue representing the model underestimation and red representing the**
 364 **model overestimation. The dotted lines in the subgraph are 1:1 line.**

365 3.2 Gross primary productivity simulation

366 Since the PFTs simulated in LPJ-GUESS model include not only BNS, IBS&TeBS
 367 and Shrubs, but also evergreen plants and grass (no development was made to its
 368 phenological simulation in the present study), we found that clear differences between

369 two versions of the model mainly appeared in the regions dominated by these deciduous
370 PFTs with improved phenological modules. We only found small differences in the
371 regions dominated by evergreen or grassland (Fig. 4c). It is also clear that the original
372 LPJ-GUESS generally simulated higher GPP than the extended one over the study
373 period, except for the IBS&TeBS dominated regions, where higher GPP from the
374 original model can be only found from 1979 to 2000 (Fig. 4d-f). By comparing multiple
375 years' monthly mean GPP values, it becomes evident that the extended phenology also
376 influences the seasonal dynamics of GPP. In regions dominated by BNS, the differences
377 in monthly GPP are primarily noticeable during spring (using extended phenological
378 module resulted in a -34.9% lower GPP in May compared to original phenological
379 module, when not specifically stated, the value is that the extended model differs from
380 the original model, Fig. 4g). In regions dominated by IBS&TeBS, GPP differs in both
381 spring (-2.8%) and autumn (-6.3%) and the difference is larger in autumn, which mainly
382 contribute to annually GPP difference (Fig. 4h). In Shrubs dominate regions, we found
383 differences in GPP in all months (-43.9%), especially in the non-growing season,
384 indicating that some evergreen plants still exist in the region when the original
385 phenological module is used, and that changes in vegetation phenology seems
386 substantially affect vegetation composition in this region (Fig. 4i). Compared with
387 VPM GPP products, we also found that LPJ-GUESS simulated GPP overestimate but
388 spatial pattern is consistent with VPM GPP products and extended LPJ-GUESS model
389 could simulate GPP more accurately during transition periods (Fig. S5 and S6).

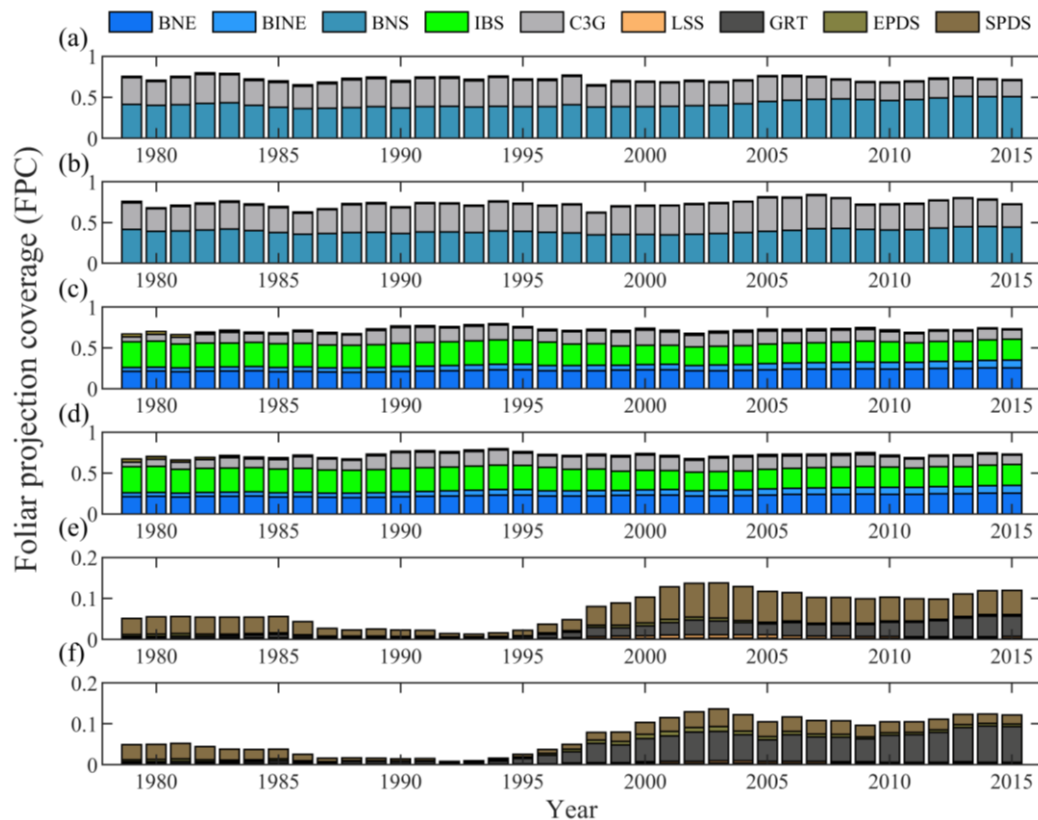


390 **Figure 4 Comparison of gross primary productivity (GPP) simulations**
 391 **between scenarios which used original phenological module and extended**
 392 **(DORMPHOT and DM) phenological module.** (a) Scenario used original
 393 phenological module, (b) scenario used extended phenological module, and (c) the
 394 difference between the two scenarios mentioned above, blue represents a larger
 395 simulation value for the LPJ-GUESS model using the original phenological module,
 396 and red is smaller. (d-f) Annual average GPP for BNS, IBS&TeBS and Shrubs PFTs
 397 from 1979 to 2015. (g-i) Multi-year mean monthly GPP for BNS, IBS&TeBS and
 398 Shrubs PFTs from 1979 to 2015.

399

400 The potential natural plant distribution also confirmed that the gridcells with large
 401 differences in phenological simulations between original and extended LPJ-GUESS has
 402 also large differences in dominant vegetation types (Fig. S3). We selected typical
 403 gridcells in BNS, IBS&TeBS and Shrubs region, and compared their multi-year
 404 variation pattern of FPC, it was found that phenological changes had a clearly influence
 405 on FPC changes in BNS and Shrubs region (Fig. 5). However, in the IBS&TeBS region

406 (the gridcell dominated by IBS was selected here), although we found that the
 407 difference in phenological simulation effects little on FPC components, due to the close
 408 proportion of IBS and BNE (fierce competition), small changes in FPC components
 409 could also lead to changes in dominant vegetation types (Fig. 5c, d).

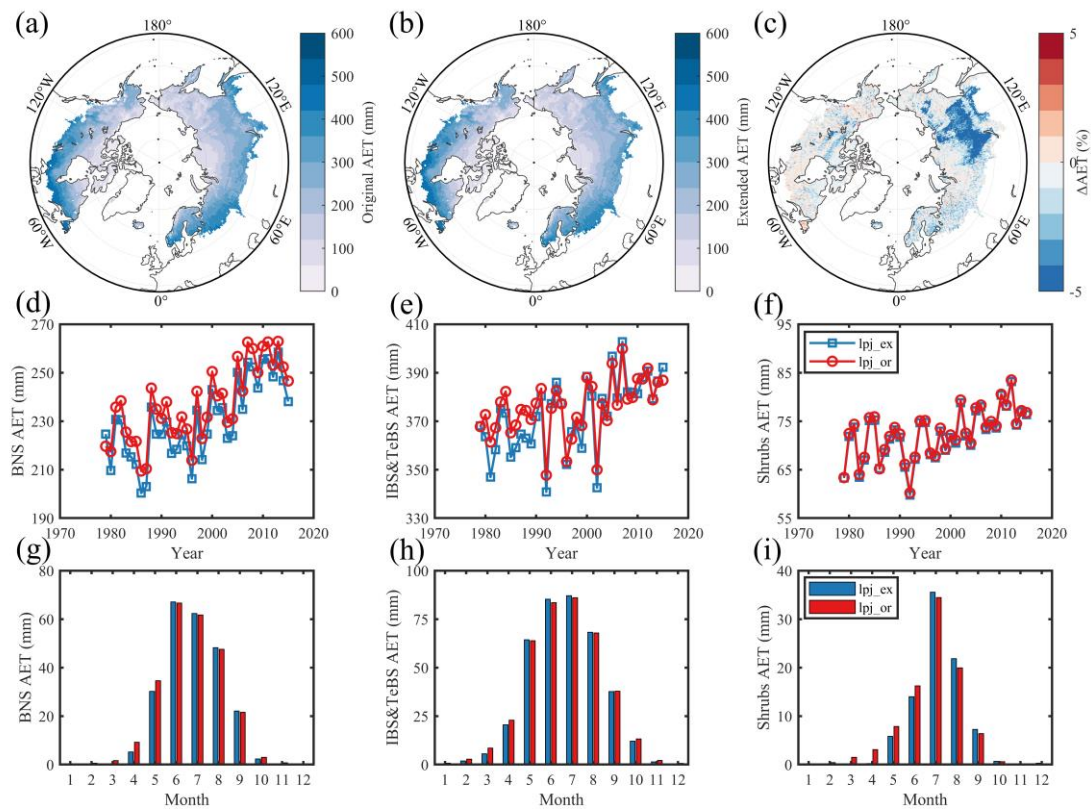


410
 411 **Figure 5. Shifts of foliage projection coverage (FPC) of typical gridcell in the**
 412 **regions dominated by BNS, IBS & TeBS and Shrubs PFTs over the period 1979 -**
 413 **2015. (a) BNS, (c) IBS&TeBS and (e) Shrubs typical gridcells used original LPJ-**
 414 **GUESS model, (b) BNS, (d) IBS&TeBS and (f) Shrubs typical gridcells used extended**
 415 **LPJ-GUESS model.**

416 3.3 Evapotranspiration simulation

417 By comparing the spatial pattern, we found that LPJ-GUESS simulated AET
 418 spatial pattern is consistent with REA ET products and BNS dominated the regions with
 419 large differences in the modelled AET under the two runs, and the simulation result
 420 using the original phenological module were larger by 3.9% compared with that using

421 the modified module (Fig.6c and S7). In the IBS&TeBS dominated region, like GPP,
 422 we found that the scenario using the original phenological module presented a larger
 423 AET during the period 1979-2000, and the two scenarios simulated AET in the Shrubs
 424 dominated region were very close (Fig. 6e-f). The seasonal dynamic patterns of AET in
 425 BNS, IBS&TeBS and Shrubs dominated regions are similar. The AET simulations get
 426 higher in spring and get lower in summer, and only in the Shrubs dominated region, the
 427 AET simulation get lower in autumn when the original phenology module is used (Fig.
 428 6g-i).



429

430 **Figure 6 Comparison of actual evapotranspiration simulations between scenarios**
 431 **which used original phenological module and extended (DORMPHOT and DM)**
 432 **phenological module.** (a) Scenario used original phenological module, (b) scenario
 433 used extended phenological module, and (c) the difference between the two scenarios
 434 mentioned above, blue represents a larger simulation value for the LPJ-GUESS model
 435 using the original phenological module, and red is smaller. (d-f) Annual average AET
 436 for BNS, IBS&TeBS and Shrubs PFTs from 1979 to 2015. (g-i) Multi-year mean

437 monthly AET for BNS, IBS&TeBS and Shrubs PFTs from 1979 to 2015.

438 **4. Discussion**

439 **4.1 Remote Sensing Phenology Facilitates Mixed-Pixel Phenology Modeling**

440 Whether through dynamic global vegetation model simulation or satellite remote
441 sensing extraction, a key issue in large-scale vegetation phenology research is the scale
442 transformation of phenology data in mixed pixels. For phenological extraction based
443 on satellite remote sensing, which is a top-down approach, the spring phenology
444 extracted from the mixed pixel (without specific dominant vegetation types) is the
445 information about the dates when the earliest plant leaf-out occurs in the pixel, while
446 the autumn phenology is the last one to senescence (Chen et al., 2018; Reed et al., 1994;
447 White et al., 2009; Fu et al., 2014). Furthermore, previous studies also have detected
448 temporal lags between phenology of NDVI, LAI and GPP, especially in tropical regions,
449 the saturation of optical vegetation indices, such as NDVI and LAI can be limited the
450 extraction of phenology, while SIF (solar-induced chlorophyll fluorescence) data could
451 overcome this issue (Guan et al., 2015; Li et al., 2021; Hmimina et al., 2013). In
452 addition, the greenness of understory phenology (low shrub or grass in forests) further
453 complicates the detecting of overstory signal (Ahl et al., 2006; Tremblay and Larocque,
454 2001). It is challenging to separate remote sensing signals into different components by
455 filtering or decoupling methods. The more feasible method is to detect phenological
456 changes with a few mixed species at a small spatial scale and conducting climate-
457 controlled experiments (Wolkovich et al., 2012).

458 DGVM-based phenological simulation is based on a bottom-up method, different

459 from phenological extraction based on remote sensing. Many studies have investigated
460 phenological models based on remote sensing data, and ignore the influence of mixed
461 pixels (Keenan and Richardson, 2015; White et al., 1997), which lacks extensibility and
462 robustness under changing circumstances, e.g. climate change. DGVMs through
463 simulating plant individuals' growth, development and senescence in the gridcell,
464 which represents different signals in the mixed pixels, and finally synthesizes the
465 vegetation signals of the whole gridcell (Sitch et al., 2003). In this study, based on top-
466 down remote sensing phenology and parameter calibrations for several relatively pure
467 pixels with clear dominance of BNS, IBS&TeBS and Shrubs PFTs, we integrated this
468 newly calibrated phenology module at PFT level into the LPJ-GUESS to reproduce the
469 gridcell-level vegetation phenology for the mixed pixels. The simulation of vegetation
470 phenology for mixed pixels enables the capture of phenological variability arising from
471 dynamic vegetation changes, as opposed to the predefined approach reliant on specific
472 pixel vegetation types, which also partly explains why phenological models based on
473 predefined vegetation types are difficult to generalize spatially (Chen et al., 2018).
474 Leveraging the advantages of wide-ranging remote sensing phenological monitoring
475 and stable monitoring frequencies, analyzing the relationship between pixel
476 constituents and vegetation signals, especially in cases where pixel constituents are
477 relatively uniform, can enhance the accuracy of phenological simulation for mixed
478 pixels.

479 **4.2 Influence of phenological shifts on ecosystem structure**

480 Our results showed that LPJ-GUESS model which using original phenological

481 module estimated earlier SOS in BNS, IBS&TeBS and Shrubs dominant regions than
482 that using the extended phenological module (Fig.3). Earlier spring phenology, which
483 is closely related to plant growth and development and has a strong influence on
484 interspecific competition (Roberts et al., 2015; Rollinson and Kaye, 2012), also lead to
485 a larger dominant area (Fig. S3). In high latitude regions, plants gain a competitive
486 niche through the advancement of spring phenology if there is no damaged tissue and
487 shoots induced by late frost and the weight of late snow fall (Augspurger, 2009; Bigler
488 and Bugmann, 2018; Drepper et al., 2022; Liu et al., 2018b). This advancement is
489 mediated by the early snowmelt synergistic changes of soil temperature and soil water
490 content. It manifested in a wider window of high resource availability and low
491 competition (Zheng et al., 2022). During this window period, plants can get more light,
492 water and nutrient resources, and then carry out vegetative growth earlier, and finally
493 increase the leaf area in the spring. As the community develops, changes in competitive
494 relations at the species or functional group level in the spring will induce to changes in
495 community composition (Morisette et al., 2009; Forrest et al., 2010). In the context of
496 climate change, differences in the phenological responses of different species may
497 further affect the distribution of species, and the inaccuracy of future phenological
498 dynamic simulations of different vegetation types in DGVMs will introduce great
499 uncertainty to the estimation of future potential natural plant distribution (Dijkstra et
500 al., 2011).

501 **4.3 Further development of phenological models**

502 Although we have substantially improved the LPJ-GUESS' accuracy of simulating

503 vegetation phenology by coupling calibrated spring (DORMPHT) and autumn (DM)
504 phenological algorithms at PFT levels, we still see the discrepancy in the grass
505 dominated regions, which owing to we did not employ the temperature and photoperiod
506 phenological model for grassland phenology simulation, because many studies indicate
507 that grassland phenology is also regulated by precipitation (Fu et al., 2021).
508 Furthermore, the current phenology algorithms only consider the synergistic effects of
509 temperature and photoperiod, but can be further linked to plant growth and physiology
510 (Fu et al., 2020; Zohner et al., 2023). In different regions (under different external
511 conditions), the driving mechanism and effective driving factors of vegetation
512 phenology process can be different. Temperature is an important factor regulating
513 phenology in energy limited regions, while water supply (precipitation, soil moisture
514 etc.) control cannot be ignored in water limited regions (Prevéy et al., 2017; Fu et al.,
515 2022). For further developing phenological module in DGVMs, on the one hand, it is
516 necessary to carry out mechanism research of phenology of different species through
517 controlled experiments, to the end of improving the existing mechanism model. On the
518 other hand, it is necessary to introduce new methods, such as machine learning, for the
519 accurate generalization of some complex key nonlinear processes (Fu et al., 2020; Dai
520 et al., 2023). Through the above two aspects of work, a comprehensive phenological
521 module can be provided for further improving the accuracy of DGVM models in
522 simulating the phenological dynamics of different PFTs in different environments.

523 **5. Conclusion**

524 In this study, we parameterized and constructed spring (DORMPHOT) and autumn

525 (DM) phenology models for BNS, IBS&TeBS and Shrubs PFTs based on the remote
526 sensing-extracted phenology data. These parameterized DORMPHOT and DM
527 algorithms were further coupled into the LPJ-GUESS model, and the results showed
528 that LPJ-GUESS using the extended phenological module substantially improved in
529 accuracy of spring and autumn phenology compared to the original phenological
530 module. Furthermore, we found that differences in phenological estimations can have
531 nonnegligible effects on carbon and water cycling processes by influencing plant annual
532 growth dynamics and ecosystem structure functions. For the carbon cycle, the influence
533 of phenological differences on BNS- and Shrubs-dominated regions was greater than
534 that of IBS&TeBS dominated regions, and there were differences in the seasonality of
535 monthly GPP simulations with different PFTs. For the water cycle, the AET simulations
536 get higher in spring and get lower in summer, and only in the Shrubs dominated region,
537 the AET simulation get lower in autumn when the original phenology module is used.
538 We highlighted the importance of phenology estimation and its process interactions in
539 DGVMs and propose further developments in vegetation phenology modeling to
540 improve the accuracy of DGVM models in simulating the phenological dynamics and
541 terrestrial carbon and water cycles.

542 **Code and data availability**

543 LPJ-GUESS is tested, refined, and developed by a global research community, but
544 the model code is managed and maintained by the Department of Physical Geography
545 and Ecosystem Science, Lund University, Sweden. The code version used for this study
546 is stored in a central code repository and can be downloaded from
547 <https://doi.org/10.5281/zenodo.10416649>. Additional details can be obtained by
548 contacting the corresponding author. Details of relevant driving data and comparison
549 data can be obtained from the data description section in this paper.

550 **Declaration of Competing Interest**

551 The authors declare that there are no known competing financial interests or
552 personal relationships that influenced the work reported in this paper.

553

554 **Acknowledgments**

555 This study was supported by the International Cooperation and Exchanges NSFC-
556 STINT (42111530181), the Distinguished Young Scholars (42025101) and the 111
557 Project (B18006). J.T. is supported by Villum Young Investigator (Grant No. 53048),
558 Swedish FORMAS (Forskningsråd för hållbar utveckling) mobility Grant (2016-01580)
559 Lund University strategic research area MERG and European Union's Horizon 2020
560 research and innovation programme under Marie Skłodowska-Curie (Grant 707187).
561 S.C., J.T. and Y.H.F. thank the Joint China-Sweden Mobility Program (Grant No.
562 CH2020-8656). We appreciate the reviewers' constructive comments and helpful

563 suggestions.

564 **Author contributions**

565 YHF and JT conceived the ideas and designed the methodology; JT provided the
566 modelling help for the LPJ-GUESS and participated in result interpretation and writing;
567 SZC modified LPJ-GUESS according to the scheme design and analyzed the data, and
568 YHF led the writing of the manuscript in corporation with SZC and JT; All authors
569 contributed critically to the drafts and gave final approval for publication.

570

571 **Reference**

- 572 Ahl, D. E., Gower, S. T., Burrows, S. N., Shabanov, N. V., Myneni, R. B., and Knyazikhin, Y.: Monitoring
573 spring canopy phenology of a deciduous broadleaf forest using MODIS, *Remote Sensing of Environment*,
574 104, 88-95, 2006.
- 575 Augspurger, C. K.: Spring 2007 warmth and frost: phenology, damage and refoliation in a temperate
576 deciduous forest, *Funct. Ecol.*, 23, 1031-1039, 2009.
- 577 Badeck, F. W., Bondeau, A., Böttcher, K., Doktor, D., Lucht, W., Schaber, J., and Sitch, S.: Responses of
578 spring phenology to climate change, *New Phytol.*, 162, 295-309, 2004.
- 579 Bartholome, E. and Belward, A. S.: GLC2000: a new approach to global land cover mapping from Earth
580 observation data, *Int. J. Remote Sens.*, 26, 1959-1977, 2005.
- 581 Bigler, C. and Bugmann, H.: Climate-induced shifts in leaf unfolding and frost risk of European trees
582 and shrubs, *Sci. Rep.*, 8, 9865, 2018.
- 583 Caffarra, A., Donnelly, A., and Chuine, I.: Modelling the timing of *Betula pubescens* budburst. II.
584 Integrating complex effects of photoperiod into process-based models, *Climate research*, 46, 159-170,
585 2011.
- 586 Cao, S., Li, M., Zhu, Z., Zha, J., Zhao, W., Duanmu, Z., Chen, J., Zheng, Y., and Chen, Y.:
587 Spatiotemporally consistent global dataset of the GIMMS Leaf Area Index (GIMMS LAI4g) from 1982
588 to 2020, *Earth System Science Data Discussions*, 1-31, 2023.
- 589 Chen, S., Fu, Y. H., Hao, F., Li, X., Zhou, S., Liu, C., and Tang, J.: Vegetation phenology and its
590 ecohydrological implications from individual to global scales, *Geography and Sustainability*, 2022a.
- 591 Chen, S., Fu, Y. H., Geng, X., Hao, Z., Tang, J., Zhang, X., Xu, Z., and Hao, F.: Influences of Shifted
592 Vegetation Phenology on Runoff Across a Hydroclimatic Gradient, *Front. Plant Sci.*, 12, 802664,
593 10.3389/fpls.2021.802664, 2022b.
- 594 Chen, S., Fu, Y. H., Wu, Z., Hao, F., Hao, Z., Guo, Y., Geng, X., Li, X., Zhang, X., and Tang, J.: Informing
595 the SWAT model with remote sensing detected vegetation phenology for improved modeling of
596 ecohydrological processes, *Journal of Hydrology*, 616, 128817, 2023.
- 597 Chen, X., Wang, D., Chen, J., Wang, C., and Shen, M.: The mixed pixel effect in land surface phenology:
598 A simulation study, *Remote Sensing of Environment*, 211, 338-344, 2018.
- 599 Chuine, I.: A unified model for budburst of trees, *Journal of theoretical biology*, 207, 337-347, 2000.
- 600 Chuine, I.: Why does phenology drive species distribution?, *Philosophical Transactions of the Royal
601 Society B: Biological Sciences*, 365, 3149-3160, 2010.
- 602 Cong, N., Piao, S., Chen, A., Wang, X., Lin, X., Chen, S., Han, S., Zhou, G., and Zhang, X.: Spring
603 vegetation green-up date in China inferred from SPOT NDVI data: A multiple model analysis, *Agric. For.
604 Meteorol.*, 165, 104-113, 10.1016/j.agrformet.2012.06.009, 2012.
- 605 Dai, W., Jin, H., Zhou, L., Liu, T., Zhang, Y., Zhou, Z., Fu, Y. H., and Jin, G.: Testing machine learning
606 algorithms on a binary classification phenological model, *Global Ecology and Biogeography*, 32, 178-
607 190, 2023.
- 608 Delpierre, N., Dufrêne, E., Soudani, K., Ulrich, E., Cecchini, S., Boé, J., and François, C.: Modelling
609 interannual and spatial variability of leaf senescence for three deciduous tree species in France, *Agric.
610 For. Meteorol.*, 149, 938-948, 2009.
- 611 Deng, F., Chen, J. M., Plummer, S., Chen, M., and Pisek, J.: Algorithm for global leaf area index retrieval
612 using satellite imagery, *IEEE Trans. Geosci. Remote Sens.*, 44, 2219-2229, 2006.
- 613 Dijkstra, J. A., Westerman, E. L., and Harris, L. G.: The effects of climate change on species composition,

614 succession and phenology: a case study, *Global Change Biol.*, 17, 2360-2369, 2011.

615 Drepper, B., Gobin, A., and Van Orshoven, J.: Spatio-temporal assessment of frost risks during the
616 flowering of pear trees in Belgium for 1971–2068, *Agric. For. Meteorol.*, 315, 108822, 2022.

617 Fang, J. and Lechowicz, M. J.: Climatic limits for the present distribution of beech (*Fagus L.*) species in
618 the world, *J. Biogeogr.*, 33, 1804-1819, 2006.

619 Forrest, J., Inouye, D. W., and Thomson, J. D.: Flowering phenology in subalpine meadows: Does climate
620 variation influence community co-flowering patterns?, *Ecology*, 91, 431-440, 2010.

621 Fu, Y., Li, X., Zhou, X., Geng, X., Guo, Y., and Zhang, Y.: Progress in plant phenology modeling under
622 global climate change, *Science China Earth Sciences*, 63, 1237-1247, 2020.

623 Fu, Y. H., Piao, S., Op de Beeck, M., Cong, N., Zhao, H., Zhang, Y., Menzel, A., and Janssens, I. A.:
624 Recent spring phenology shifts in western Central Europe based on multiscale observations, *Global
625 Ecol. Biogeogr.*, 23, 1255-1263, 2014.

626 Fu, Y. H., Geng, X., Chen, S., Wu, H., Hao, F., Zhang, X., Wu, Z., Zhang, J., Tang, J., and Vitasse, Y.:
627 Global warming is increasing the discrepancy between green (actual) and thermal (potential) seasons of
628 temperate trees, *Global Change Biology*, 29, 1377-1389, 2023.

629 Fu, Y. H., Li, X., Chen, S., Wu, Z., Su, J., Li, X., Li, S., Zhang, J., Tang, J., and Xiao, J.: Soil moisture
630 regulates warming responses of autumn photosynthetic transition dates in subtropical forests, *Global
631 Change Biol.*, 28, 4935-4946, 2022.

632 Fu, Y. H., Zhou, X., Li, X., Zhang, Y., Geng, X., Hao, F., Zhang, X., Hanninen, H., Guo, Y., and De
633 Boeck, H. J.: Decreasing control of precipitation on grassland spring phenology in temperate China,
634 *Global Ecol. Biogeogr.*, 30, 490-499, 2021.

635 Geng, X., Zhou, X., Yin, G., Hao, F., Zhang, X., Hao, Z., Singh, V. P., and Fu, Y. H.: Extended growing
636 season reduced river runoff in Luanhe River basin, *Journal of Hydrology*, 582, 124538, 2020.

637 Guan, K., Pan, M., Li, H., Wolf, A., Wu, J., Medvigy, D., Caylor, K. K., Sheffield, J., Wood, E. F., and
638 Malhi, Y.: Photosynthetic seasonality of global tropical forests constrained by hydroclimate, *Nat. Geosci.*,
639 8, 284-289, 2015.

640 Hänninen, H.: Modelling bud dormancy release in trees from cool and temperate regions, 1990.

641 Hickler, T., Smith, B., Sykes, M. T., Davis, M. B., Sugita, S., and Walker, K.: Using a generalized
642 vegetation model to simulate vegetation dynamics in northeastern USA, *Ecology*, 85, 519-530, 2004.

643 Hmimina, G., Dufrêne, E., Pontailier, J.-Y., Delpierre, N., Aubinet, M., Caquet, B., De Grandcourt, A.,
644 Burban, B., Flechard, C., and Granier, A.: Evaluation of the potential of MODIS satellite data to predict
645 vegetation phenology in different biomes: An investigation using ground-based NDVI measurements,
646 *Remote Sens. Environ.*, 132, 145-158, 2013.

647 Huang, M., Piao, S., Janssens, I. A., Zhu, Z., Wang, T., Wu, D., Ciais, P., Myneni, R. B., Peaucelle, M.,
648 and Peng, S.: Velocity of change in vegetation productivity over northern high latitudes, *Nat. Ecol. Evol.*,
649 1, 1649-1654, 2017.

650 Jain, A. K. and Yang, X.: Modeling the effects of two different land cover change data sets on the carbon
651 stocks of plants and soils in concert with CO₂ and climate change, *Global Biogeochem. Cycles*, 19, 2005.

652 Kaufmann, R. K., Zhou, L., Knyazikhin, Y., Shabanov, V., Myneni, R. B., and Tucker, C. J.: Effect of
653 orbital drift and sensor changes on the time series of AVHRR vegetation index data, *IEEE Trans. Geosci.
654 Remote Sens.*, 38, 2584-2597, 2000.

655 Keenan, T. F. and Richardson, A. D.: The timing of autumn senescence is affected by the timing of spring
656 phenology: implications for predictive models, *Global Change Biol.*, 21, 2634-2641, 2015.

657 Keenan, T. F., Gray, J., Friedl, M. A., Toomey, M., Bohrer, G., Hollinger, D. Y., Munger, J. W., O'Keefe,

658 J., Schmid, H. P., SueWing, I., Yang, B., and Richardson, A. D.: Net carbon uptake has increased through
659 warming-induced changes in temperate forest phenology, *Nat. Clim. Change*, 4, 598-604,
660 10.1038/Nclimate2253, 2014.

661 Kim, J. H., Hwang, T., Yang, Y., Schaaf, C. L., Boose, E., and Munger, J. W.: Warming-induced earlier
662 greenup leads to reduced stream discharge in a temperate mixed forest catchment, *J. Geophys. Res.:
663 Biogeosci.*, 123, 1960-1975, 2018.

664 Kramer, K.: Selecting a model to predict the onset of growth of *Fagus sylvatica*, *J. Appl. Ecol.*, 172-181,
665 1994.

666 Krinner, G., Viovy, N., de Noblet-Ducoudré, N., Ogée, J., Polcher, J., Friedlingstein, P., Ciais, P., Sitch,
667 S., and Prentice, I. C.: A dynamic global vegetation model for studies of the coupled atmosphere-
668 biosphere system, *Global Biogeochem. Cycles*, 19, 2005.

669 Kucharik, C. J., Barford, C. C., El Maayar, M., Wofsy, S. C., Monson, R. K., and Baldocchi, D. D.: A
670 multiyear evaluation of a Dynamic Global Vegetation Model at three AmeriFlux forest sites: Vegetation
671 structure, phenology, soil temperature, and CO₂ and H₂O vapor exchange, *Ecol. Modell.*, 196, 1-31,
672 2006.

673 Li, X., Fu, Y. H., Chen, S., Xiao, J., Yin, G., Li, X., Zhang, X., Geng, X., Wu, Z., and Zhou, X.: Increasing
674 importance of precipitation in spring phenology with decreasing latitudes in subtropical forest area in
675 China, *Agricultural and Forest Meteorology*, 304, 108427, 2021.

676 Liu, Q., Fu, Y. H., Liu, Y., Janssens, I. A., and Piao, S.: Simulating the onset of spring vegetation growth
677 across the Northern Hemisphere, *Global Change Biol.*, 24, 1342-1356, 2018a.

678 Liu, Q., Piao, S., Janssens, I. A., Fu, Y., Peng, S., Lian, X., Ciais, P., Myneni, R. B., Peñuelas, J., and
679 Wang, T.: Extension of the growing season increases vegetation exposure to frost, *Nature
680 communications*, 9, 426, 2018b.

681 Lu, J., Wang, G., Chen, T., Li, S., Hagan, D. F. T., Kattel, G., Peng, J., Jiang, T., and Su, B.: A harmonized
682 global land evaporation dataset from model-based products covering 1980–2017, *Earth Syst. Sci. Data*,
683 13, 5879-5898, 2021.

684 Marini, F. and Walczak, B.: Particle swarm optimization (PSO). A tutorial, *Chemometrics and Intelligent
685 Laboratory Systems*, 149, 153-165, 2015.

686 Medvigy, D., Wofsy, S., Munger, J., Hollinger, D., and Moorcroft, P.: Mechanistic scaling of ecosystem
687 function and dynamics in space and time: Ecosystem Demography model version 2, *J. Geophys. Res.:
688 Biogeosci.*, 114, 2009.

689 Morales, P., Sykes, M. T., Prentice, I. C., Smith, P., Smith, B., Bugmann, H., Zierl, B., Friedlingstein, P.,
690 Viovy, N., and Sabaté, S.: Comparing and evaluating process-based ecosystem model predictions of
691 carbon and water fluxes in major European forest biomes, *Global change biology*, 11, 2211-2233, 2005.

692 Morisette, J. T., Richardson, A. D., Knapp, A. K., Fisher, J. I., Graham, E. A., Abatzoglou, J., Wilson, B.
693 E., Breshears, D. D., Henebry, G. M., and Hanes, J. M.: Tracking the rhythm of the seasons in the face
694 of global change: phenological research in the 21st century, *Front. Ecol. Environ.*, 7, 253-260, 2009.

695 Piao, S., Fang, J., Zhou, L., Ciais, P., and Zhu, B.: Variations in satellite-derived phenology in China's
696 temperate vegetation, *Global Change Biol.*, 12, 672-685, 2006.

697 Piao, S., Liu, Q., Chen, A., Janssens, I. A., Fu, Y., Dai, J., Liu, L., Lian, X., Shen, M., and Zhu, X.: Plant
698 phenology and global climate change: Current progresses and challenges, *Global change biology*, 25,
699 1922-1940, 2019.

700 Pinzon, J. E. and Tucker, C. J.: A non-stationary 1981–2012 AVHRR NDVI3g time series, *Remote Sens.*,
701 6, 6929-6960, 2014.

702 Poli, R., Kennedy, J., and Blackwell, T.: Particle swarm optimization: An overview, *Swarm Intell.*, 1, 33-
703 57, 2007.

704 Prevéy, J., Vellend, M., Rüger, N., Hollister, R. D., Bjorkman, A. D., Myers-Smith, I. H., Elmendorf, S.
705 C., Clark, K., Cooper, E. J., and Elberling, B.: Greater temperature sensitivity of plant phenology at
706 colder sites: implications for convergence across northern latitudes, *Global Change Biol.*, 23, 2660-2671,
707 2017.

708 Reed, B. C., Brown, J. F., VanderZee, D., Loveland, T. R., Merchant, J. W., and Ohlen, D. O.: Measuring
709 phenological variability from satellite imagery, *Journal of vegetation science*, 5, 703-714, 1994.

710 Richardson, A. D., Anderson, R. S., Arain, M. A., Barr, A. G., Bohrer, G., Chen, G., Chen, J. M., Ciais,
711 P., Davis, K. J., and Desai, A. R.: Terrestrial biosphere models need better representation of vegetation
712 phenology: results from the North American Carbon Program Site Synthesis, *Global Change Biology*,
713 18, 566-584, 2012.

714 Rinnan, R., Iversen, L. L., Tang, J., Vedel-Petersen, I., Schollert, M., and Schurgers, G.: Separating direct
715 and indirect effects of rising temperatures on biogenic volatile emissions in the Arctic, *Proceedings of
716 the National Academy of Sciences*, 117, 32476-32483, 10.1073/pnas.2008901117, 2020.

717 Roberts, A. M., Tansey, C., Smithers, R. J., and Phillimore, A. B.: Predicting a change in the order of
718 spring phenology in temperate forests, *Global Change Biol.*, 21, 2603-2611, 2015.

719 Rollinson, C. R. and Kaye, M. W.: Experimental warming alters spring phenology of certain plant
720 functional groups in an early successional forest community, *Global Change Biol.*, 18, 1108-1116, 2012.

721 Ryu, S.-R., Chen, J., Noormets, A., Bresee, M. K., and Ollinger, S. V.: Comparisons between PnET-Day
722 and eddy covariance based gross ecosystem production in two Northern Wisconsin forests, *Agric. For.
723 Meteorol.*, 148, 247-256, 2008.

724 Sarvas, R.: Investigations on the annual cycle of development of forest trees. Active period,
725 Investigations on the annual cycle of development of forest trees. Active period., 76, 1972.

726 Savitzky, A. and Golay, M. J.: Smoothing and differentiation of data by simplified least squares
727 procedures, *Anal. Chem.*, 36, 1627-1639, 1964.

728 Schaefer, K., Collatz, G. J., Tans, P., Denning, A. S., Baker, I., Berry, J., Prihodko, L., Suits, N., and
729 Philpott, A.: Combined simple biosphere/Carnegie-Ames-Stanford approach terrestrial carbon cycle
730 model, *J. Geophys. Res.: Biogeosci.*, 113, 2008.

731 Sellers, P., Mintz, Y., Sud, Y. e. a., and Dalcher, A.: A simple biosphere model (SiB) for use within general
732 circulation models, *J. Atmos. Sci.*, 43, 505-531, 1986.

733 Sellers, P., Randall, D., Collatz, G., Berry, J., Field, C., Dazlich, D., Zhang, C., Collelo, G., and Bounoua,
734 L.: A revised land surface parameterization (SiB2) for atmospheric GCMs. Part I: Model formulation, *J.
735 Clim.*, 9, 676-705, 1996.

736 Sitch, S., Smith, B., Prentice, I. C., Arneth, A., Bondeau, A., Cramer, W., Kaplan, J. O., Levis, S., Lucht,
737 W., and Sykes, M. T.: Evaluation of ecosystem dynamics, plant geography and terrestrial carbon cycling
738 in the LPJ dynamic global vegetation model, *Global Change Biol.*, 9, 161-185, 2003.

739 Sykes, M. T., Prentice, I. C., and Cramer, W.: A bioclimatic model for the potential distributions of north
740 European tree species under present and future climates, *Journal of Biogeography*, 203-233, 1996.

741 Tang, J., Zhou, P., Miller, P. A., Schurgers, G., Gustafson, A., Makkonen, R., Fu, Y. H., and Rinnan, R.:
742 High-latitude vegetation changes will determine future plant volatile impacts on atmospheric organic
743 aerosols, *npj Climate and Atmospheric Science*, 6, 147, 2023.

744 Thornton, P. E., Law, B. E., Gholz, H. L., Clark, K. L., Falge, E., Ellsworth, D. S., Goldstein, A. H.,
745 Monson, R. K., Hollinger, D., and Falk, M.: Modeling and measuring the effects of disturbance history

746 and climate on carbon and water budgets in evergreen needleleaf forests, *Agric. For. Meteorol.*, 113, 185-
747 222, 2002.

748 Tremblay, N. O. and Larocque, G. R.: Seasonal dynamics of understory vegetation in four eastern
749 Canadian forest types, *International Journal of Plant Sciences*, 162, 271-286, 2001.

750 Tucker, C. J., Pinzon, J. E., Brown, M. E., Slayback, D. A., Pak, E. W., Mahoney, R., Vermote, E. F., and
751 El Saleous, N.: An extended AVHRR 8-km NDVI dataset compatible with MODIS and SPOT vegetation
752 NDVI data, *Int. J. Remote Sens.*, 26, 4485-4498, 2005.

753 Viovy, N.: CRUNCEP version 7-atmospheric forcing data for the community land model, 2018.

754 White, M. A., Thornton, P. E., and Running, S. W.: A continental phenology model for monitoring
755 vegetation responses to interannual climatic variability, *Global Biogeochem. Cycles*, 11, 217-234, 1997.

756 White, M. A., de Beurs, K. M., Didan, K., Inouye, D. W., Richardson, A. D., Jensen, O. P., O'keefe, J.,
757 Zhang, G., Nemani, R. R., and van Leeuwen, W. J.: Intercomparison, interpretation, and assessment of
758 spring phenology in North America estimated from remote sensing for 1982–2006, *Global Change
759 Biology*, 15, 2335-2359, 2009.

760 Wolkovich, E. M., Cook, B. I., Allen, J. M., Crimmins, T., Betancourt, J. L., Travers, S. E., Pau, S.,
761 Regetz, J., Davies, T. J., and Kraft, N. J.: Warming experiments underpredict plant phenological
762 responses to climate change, *Nature*, 485, 494-497, 2012.

763 Zani, D., Crowther, T. W., Mo, L., Renner, S. S., and Zohner, C. M.: Increased growing-season
764 productivity drives earlier autumn leaf senescence in temperate trees, *Science*, 370, 1066-1071, 2020.

765 Zhang, Y., Commene, R., Zhou, S., Williams, A. P., and Gentine, P.: Light limitation regulates the
766 response of autumn terrestrial carbon uptake to warming, *Nat. Clim. Change*, 10, 739-743, 2020.

767 Zhang, Y., Xiao, X., Wu, X., Zhou, S., Zhang, G., Qin, Y., and Dong, J.: A global moderate resolution
768 dataset of gross primary production of vegetation for 2000–2016, *Sci. Data*, 4, 1-13, 2017.

769 Zheng, J., Jia, G., and Xu, X.: Earlier snowmelt predominates advanced spring vegetation greenup in
770 Alaska, *Agricultural and Forest Meteorology*, 315, 108828, 2022.

771 Zhou, X., Geng, X., Yin, G., Hänninen, H., Hao, F., Zhang, X., and Fu, Y. H.: Legacy effect of spring
772 phenology on vegetation growth in temperate China, *Agricultural and Forest Meteorology*, 281, 107845,
773 2020.

774 Zhu, Z., Piao, S., Myneni, R. B., Huang, M., Zeng, Z., Canadell, J. G., Ciais, P., Sitch, S., Friedlingstein,
775 P., and Arneeth, A.: Greening of the Earth and its drivers, *Nat. Clim. Change*, 6, 791-795, 2016.

776 Zohner, C. M., Mirzaghali, L., Renner, S. S., Mo, L., Rebindaine, D., Bucher, R., Palouš, D., Vitasse, Y.,
777 Fu, Y. H., and Stocker, B. D.: Effect of climate warming on the timing of autumn leaf senescence reverses
778 after the summer solstice, *Science*, 381, eadf5098, 2023.

779